Science Advances
AAAS

advances.sciencemag.org/cgi/content/full/4/10/eaat5383/DC1

Supplementary Materials for

Upgrading traditional liquid electrolyte via in situ gelation for future lithium metal batteries

Feng-Quan Liu, Wen-Peng Wang, Ya-Xia Yin, Shuai-Feng Zhang, Ji-Lei Shi, Lu Wang, Xu-Dong Zhang, Yue Zheng, Jian-Jun Zhou, Lin Li*, Yu-Guo Guo*

*Corresponding author. Email: ygguo@iccas.ac.cn (Y.-G.G.); lilinll@bnu.edu.cn (L.L.)

Published 5 October 2018, *Sci. Adv.* **4**, eaat5383 (2018)
DOI: 10.1126/sciadv.aat5383

The PDF file includes:

Other Supplementary Material for this manuscript includes the following:

(available at advances.sciencemag.org/cgi/content/full/4/10/eaat5383/DC1)

Movie S1 (.mp4 format). Contact angle measurement of polymer precursor and LE on cathode substrates.

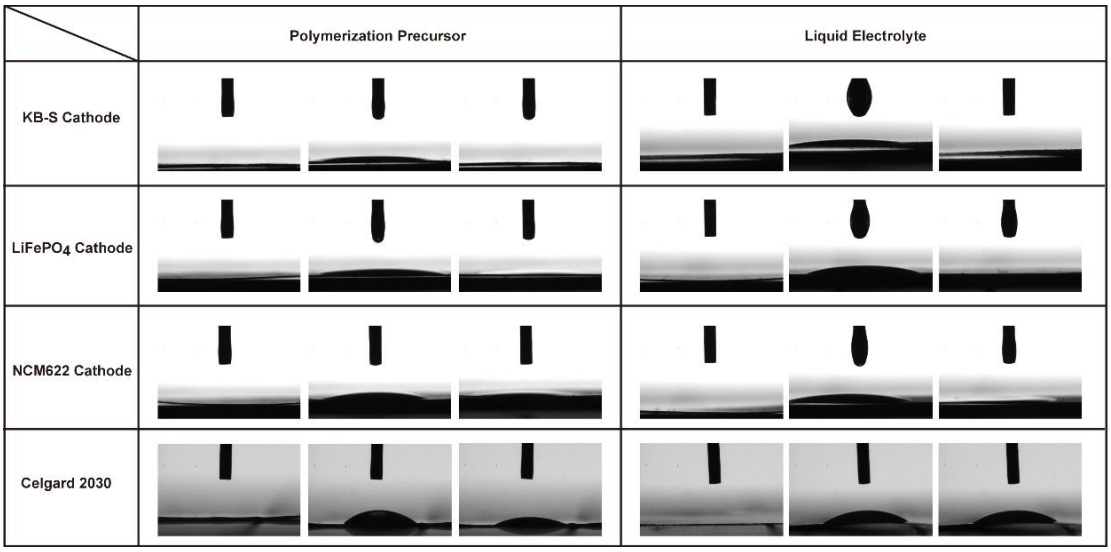

Fig. S1. Contact angle measurement of the polymer precursor and LE on the different substrates.

As the results reveal, the polymerization precursor exhibits good wettability on three different cathode substrates, which is comparable with commercial liquid electrolyte. Meanwhile, a small angle of 22.1° is detected for the precursor on Celgard separator that is also similar to the liquid electrolyte, indicating the favorable wettability of polymer precursor for separator.

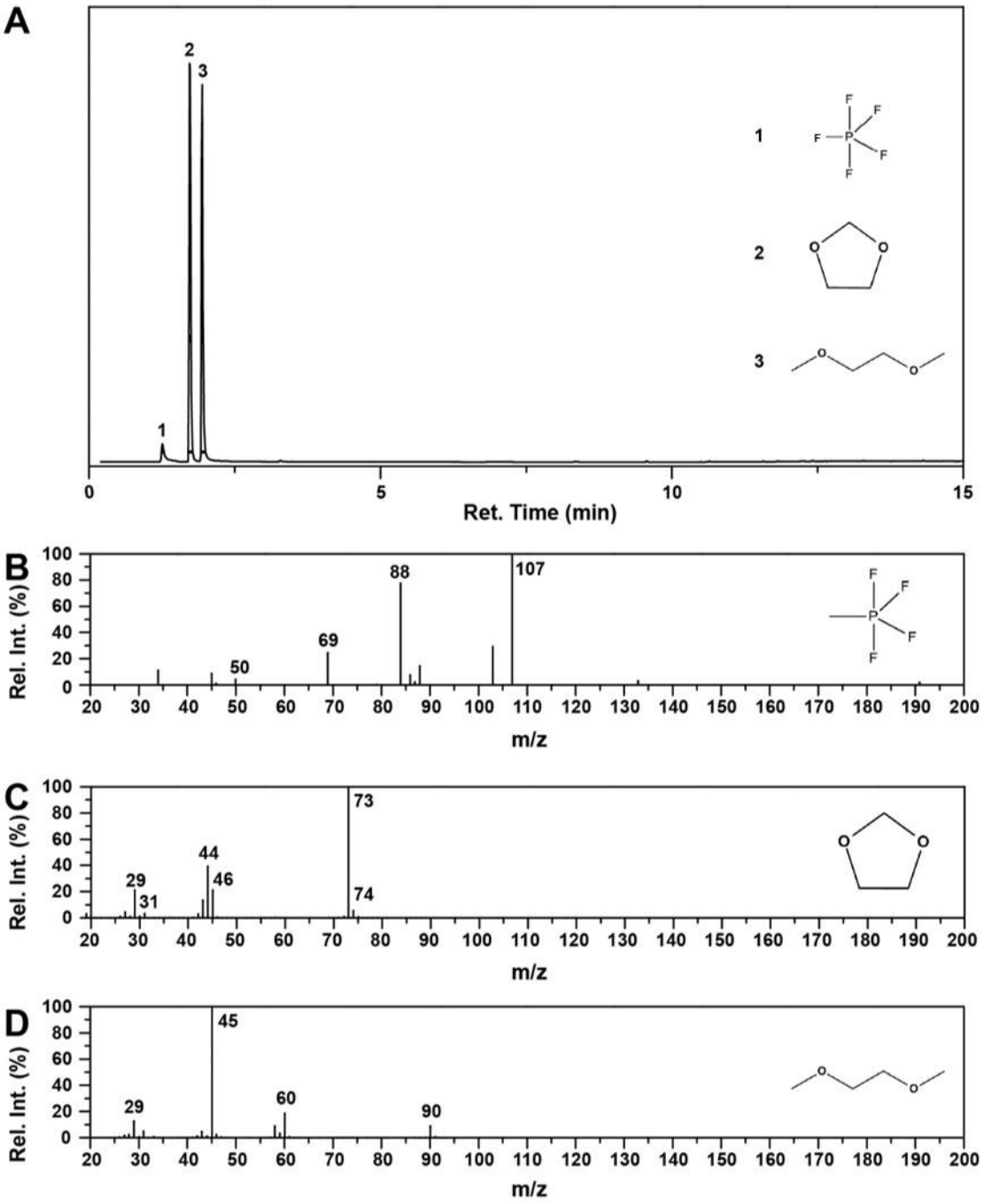

Fig. S2. GC-MS of mixed gases. (**A**) The SCAN curves of mixed gases. The MS graphs of resolved SCAN (**B**) PF_5, (**C**) DOL and (**D**) DME.

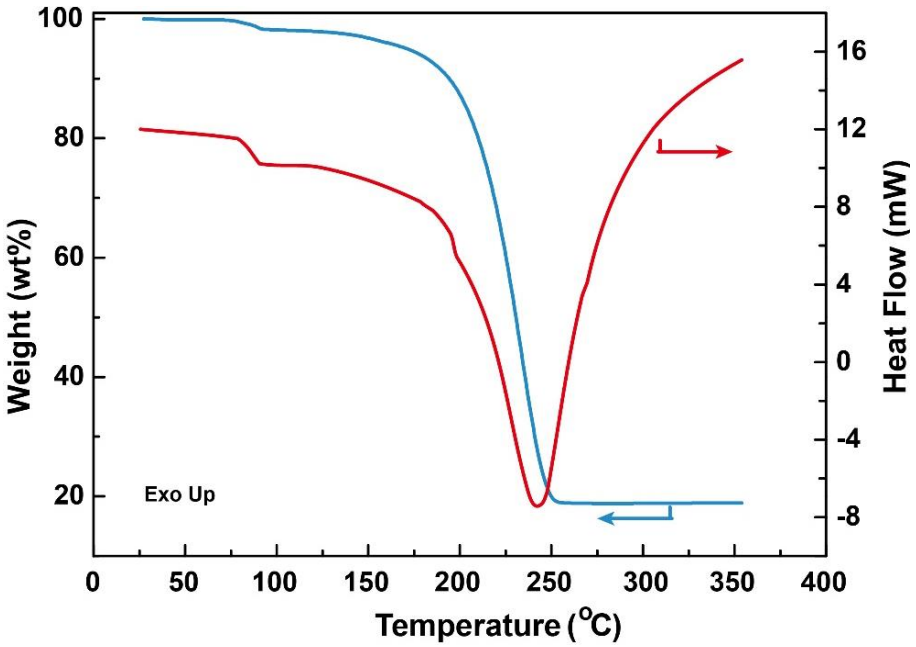

Fig. S3. Thermogravimetric analysis and differential scanning calorimetry curves of $LiPF_6$.

The TG-DSC curves of $LiPF_6$ in a temperature range of 25 ^oC ~350 ^oC at a heating rate of 40 ^oC min^{-1}.

The thermal behavior of $LiPF_6$ is exhibited in fig. S3. For thermogravimetric (TG) curve (blue line), the weight loss refers to H_2O at about 100 ^oC. The weight change of sample stops after the temperature increases to 250 ^oC. The remaining weight is about 18% of the initial sample, referring to lithium fluoride (LiF) in reserve. The results indicate that phosphorus pentafluoride (PF_5) is the only gaseous product of the thermal decomposition of $LiPF_6$. Different scanning calorimetry (DSC) curve (red line) shows that the decomposition of $LiPF_6$ is an endothermic process. There is a small endothermic peak on the main peak at 200 ^oC, which is attributed to the solid phase transformation. It also explains that the thermal decomposition of $LiPF_6$ can be promoted by the released heat in the dissolution progress.

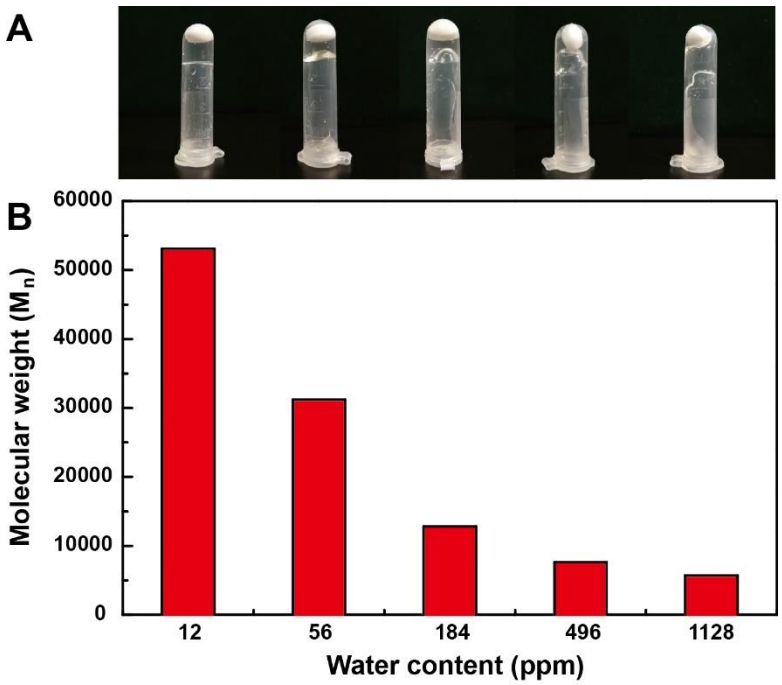

Fig. S4. Effect of H_2O content on polymerization. (**A**) The optical photographs of GPEs and (**B**) the molecular weight of polymer frameworks in GPEs with various H_2O content. Photo credit: Feng-Quan Liu, Beijing Normal University.

As the polymer chains grows to certain degree, H_2O will attack the oxonium ions and perform a nucleophilic substitution as follow.

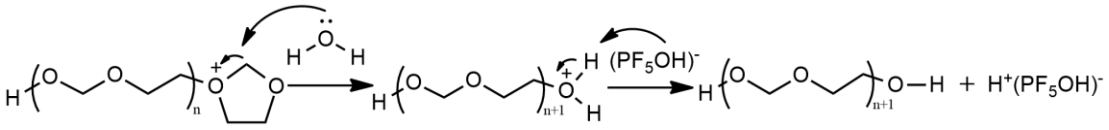

This reaction will terminate the current chain growth and release $H^+(PF_5OH)^-$ for other polymer chains. As a result, with the increase of H_2O, the opportunity of H_2O terminating chain growth becomes larger, which will cause the decrease of polymer molecular weight. To verify this point, H_2O content in the electrolyte used for polymerization is raised and it is proved that the H_2O content increment would obviously reduce the gelation rate (fig. S4A) and the polymer molecular weight (fig. S4B).

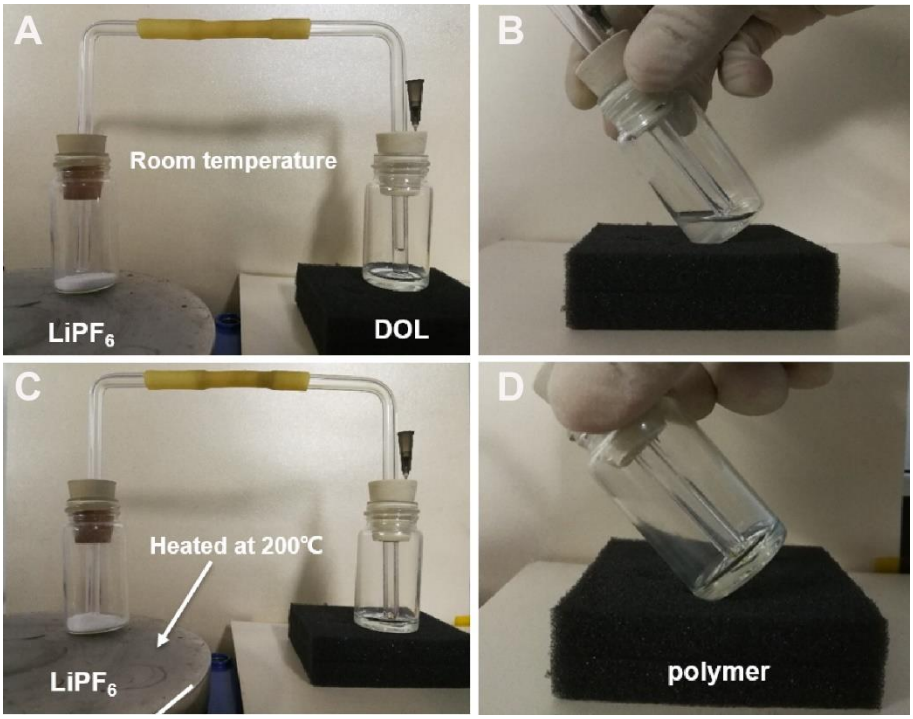

Fig. S5. Polymerization mechanism of DOL induced by $LiPF_6$. Photo credit: Wen-Peng Wang, Institute of Chemistry, Chinese Academy of Sciences.

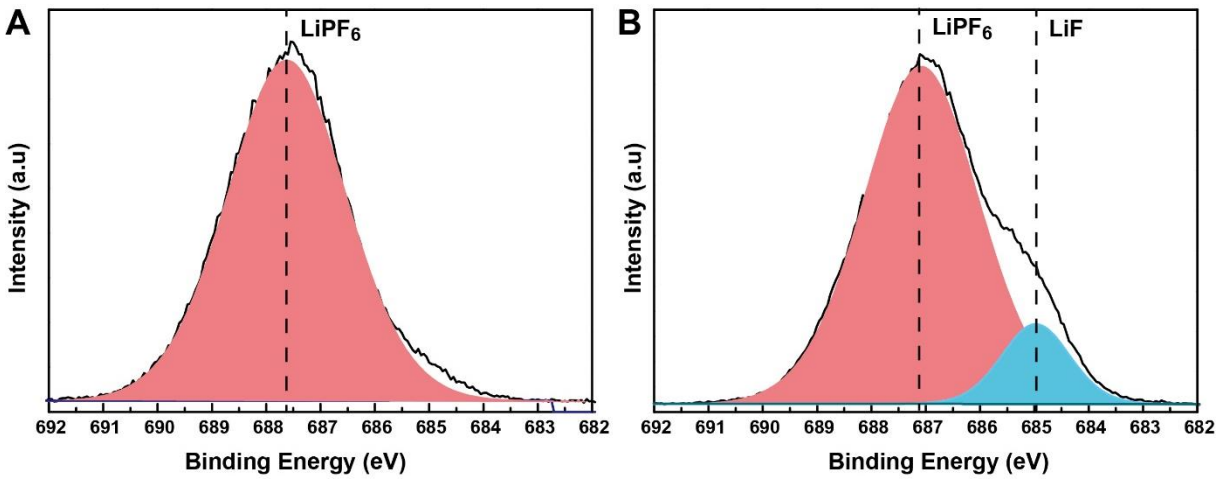

Fig. S6. XPS spectra of $LiPF_6$ and GPE. The F1s XPS of (**A**) $LiPF_6$ and (**B**) GPE.

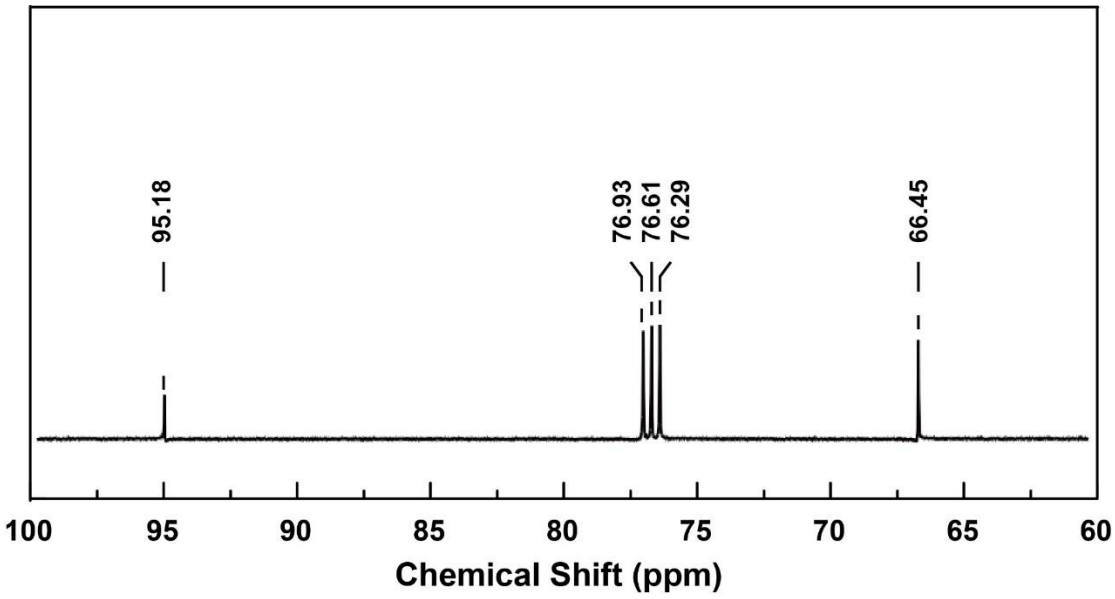

Fig. S7. ^{13}C NMR spectrum of PDXL (deuterated chloroform as solvent).

The chemical shift at 66.45 ppm corresponds to the C on group -O-CH_2-CH_2-O-, and 95.18 ppm is assigned to -O-CH_2-O-. The result is in accordance with the structure of -CH_2-O-CH_2-CH_2-O- and the corresponding ^{1}H NMR spectrum.

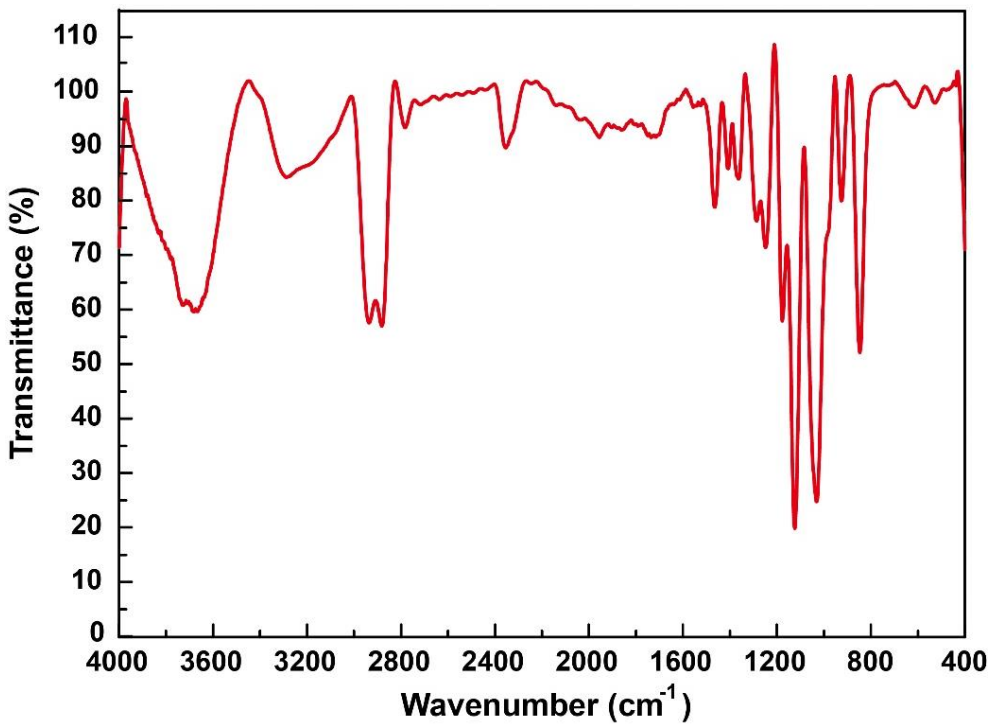

Fig. S8. FTIR spectrum of PDXL.

Fig. S8 further supports the structure illustrated and it is obvious that two mean functional groups exist in the structure of the polymer, 1100 cm^{-1} for -C-O- stretching vibration and 2900 cm^{-1} for -CH_2- stretching vibration, respectively. The characterization analysis proves that the resultant polymer (PDXL) is the linkage of the structural unit -CH_2-O-CH_2-CH_2-O-.

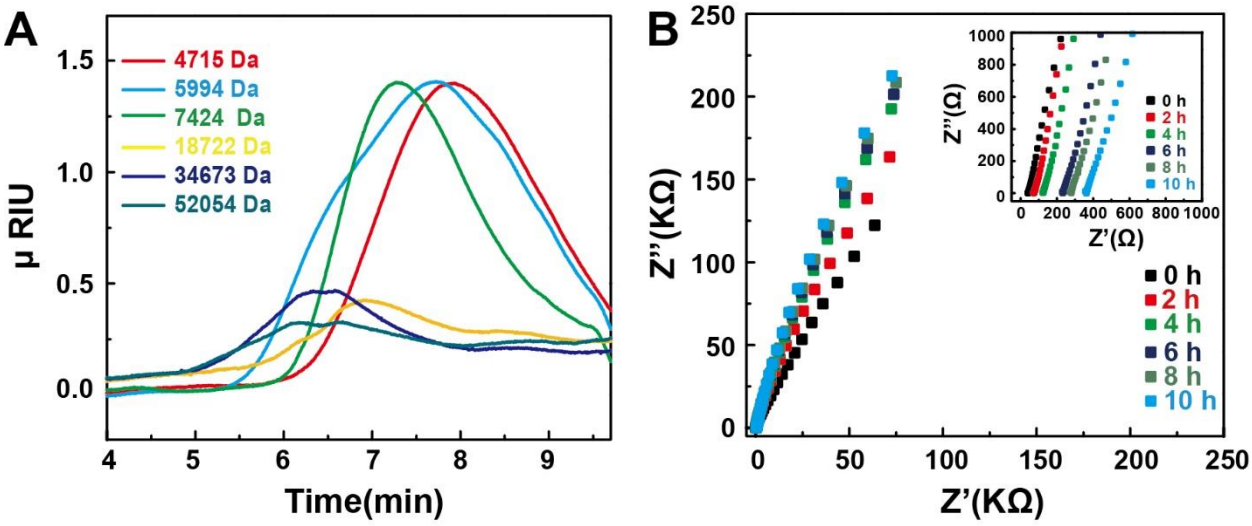

Fig. S9. Characteristic changes of GPE during the whole polymerization progress. (**A**) The molecular weight (M_n) and (**B**) the ionic conductivity evolution during the *in-situ* polymerization process of GPE with the increment of two hours.

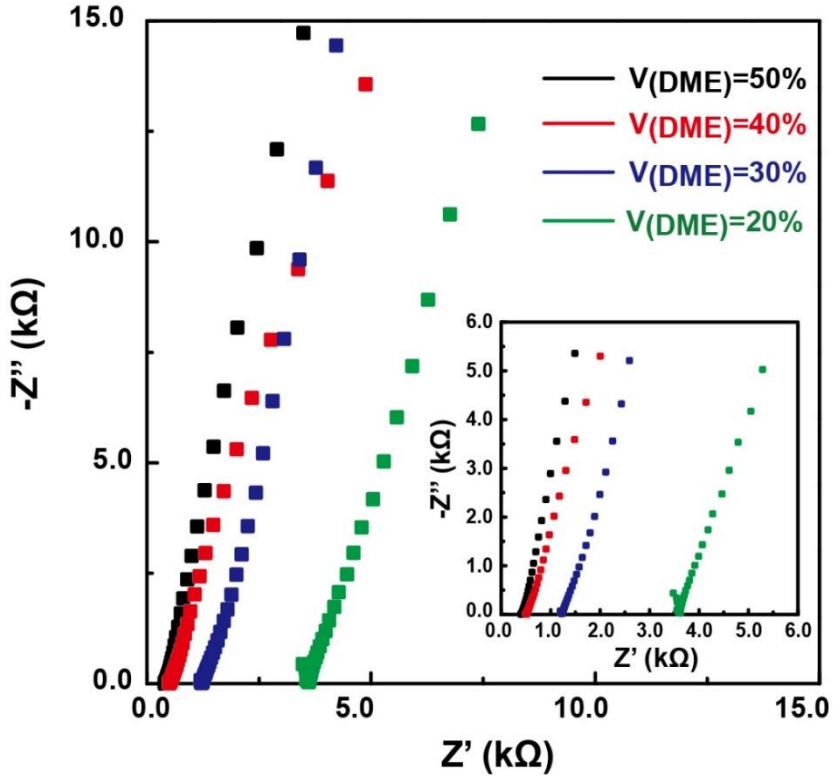

Fig. S10. EIS curves of the GPE with various DME content in the precursors.

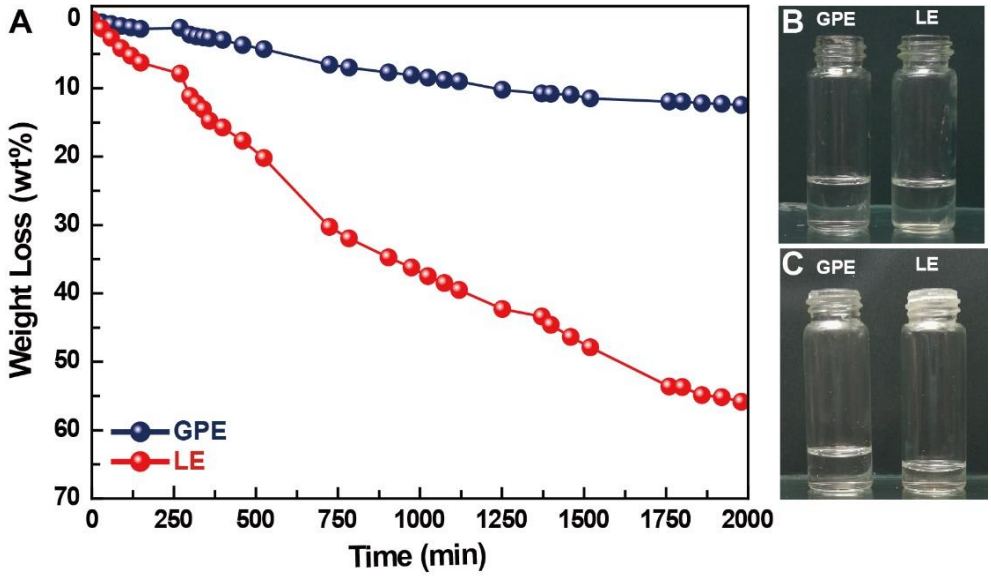

Fig. S11. Volatilization property of GPE and LE. (**A**) The curves of weight loss of GPE and LE on volatility with time. The optical photographs of bottles with GPE and LE with the same weight: (**B**) original state and (**C**) final state. Photo credit: Feng-Quan Liu, Beijing 100875, China.

Prior to illuminating the difference of the GPE and the LE on volatility, the weight loss of them in exposure over time are observed, and the results are shown in fig. S11. It can be seen that the weight of LE drops rapidly due to the violent volatility of solution components, especially DOL. The weight reduces slowly in the later stage attributed to the viscosity of electrolyte rising up. In comparison, weight loss of GPE is indistinctively perpetual, indicating the liquid DME is confined inside the polymer matrix which is also volatility inert.

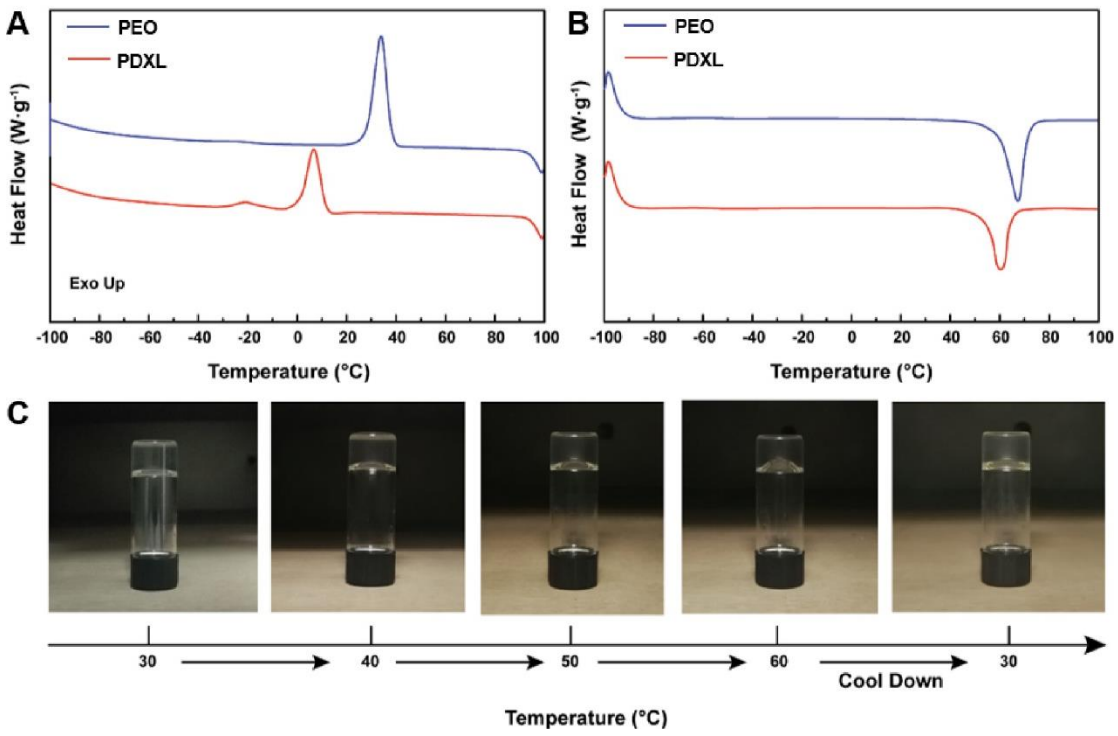

Fig. S12. Thermal analysis of the PDXL and polyethylene oxide (PEO). (**A**) The DSC curves of PDXL (red line) and PEO (blue line) during cooling. (**B**) The DSC curves of PDXL (red line) and PEO (blue line) during heating. (**C**) The optical photographs of the GPE at different temperatures. Photo credit: Wen-Peng Wang, Institute of Chemistry, Chinese Academy of Sciences.

The melting point of polymer framework can reach as high as 60 ^{o}C, which is close to PEO with the average M_w of 100000. Considering that the industrial battery formation temperature is normally below 60 ^{o}C, it can be implied that the framework could remain solid state in the regular battery formation progress. Furthermore, it is demonstrated that the integral GPE still maintains originally solid morphology without flowing tendency when placed at 30, 40 and 50 ^{o}C for 1 h respectively, and only when the temperature climbs at 60 ^{o}C, the GPE starts to soften slightly. It is also noteworthy that as the temperature is recovered to the original 30 ^{o}C, the GPE also restores the stretchy and immovable characteristics, featuring fine tolerance and reversibility for the temperature variation during battery formation process.

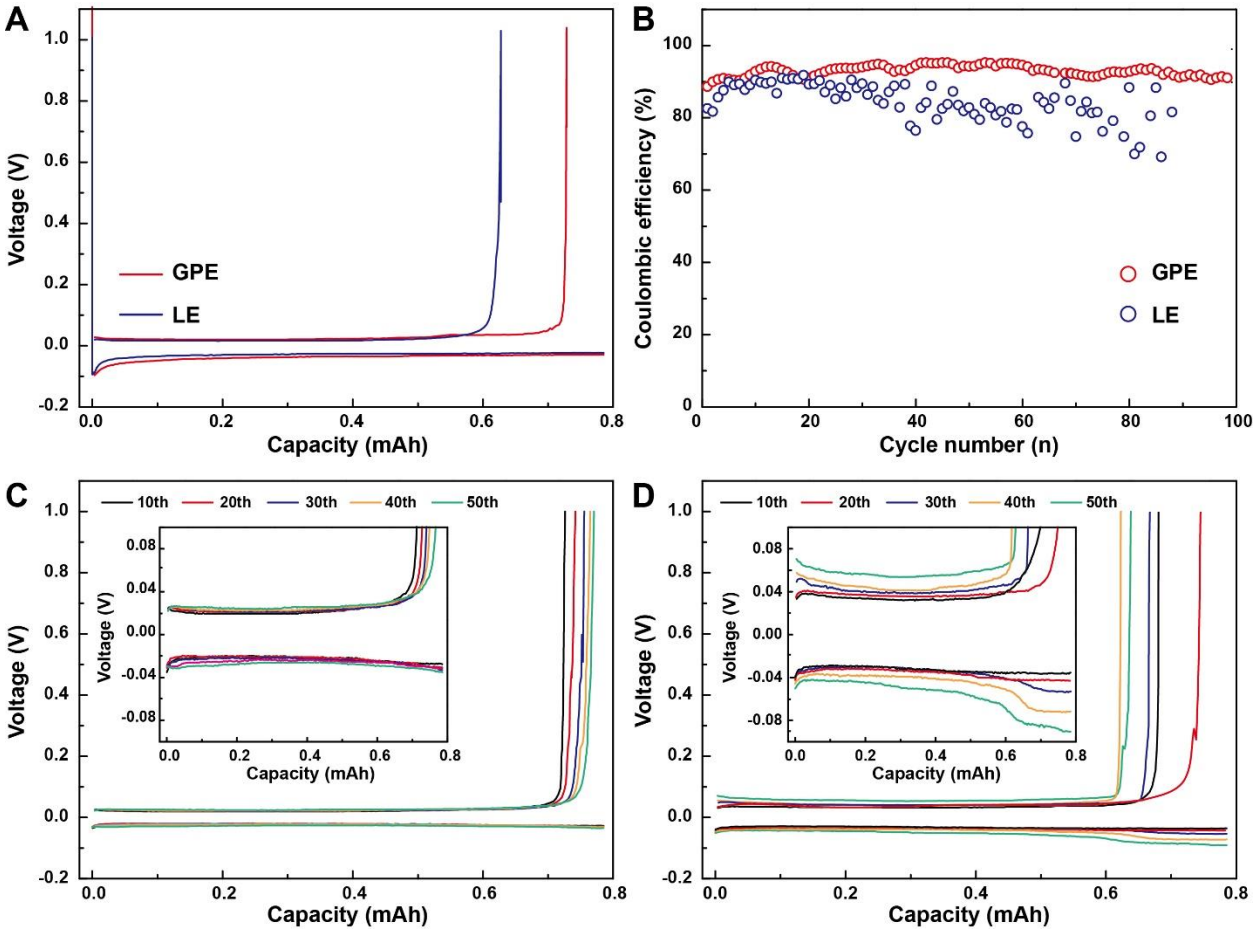

Fig. S13. Electrochemical tests of the Li-Cu batteries with GPE and LE. (**A**) The initial charge-discharge curves of the Li-Cu batteries with GPE (red curve) and LE (blue curve) at 1 mA cm^{-2}. (**B**) Coulombic efficiency of the Li-Cu batteries with GPE (red dotted line) and LE (blue dotted line) at 1 mA cm^{-2}. Voltage profiles of the Li-Cu batteries (**C**) with GPE and (**D**) with LE at 1 mA cm^{-2}.

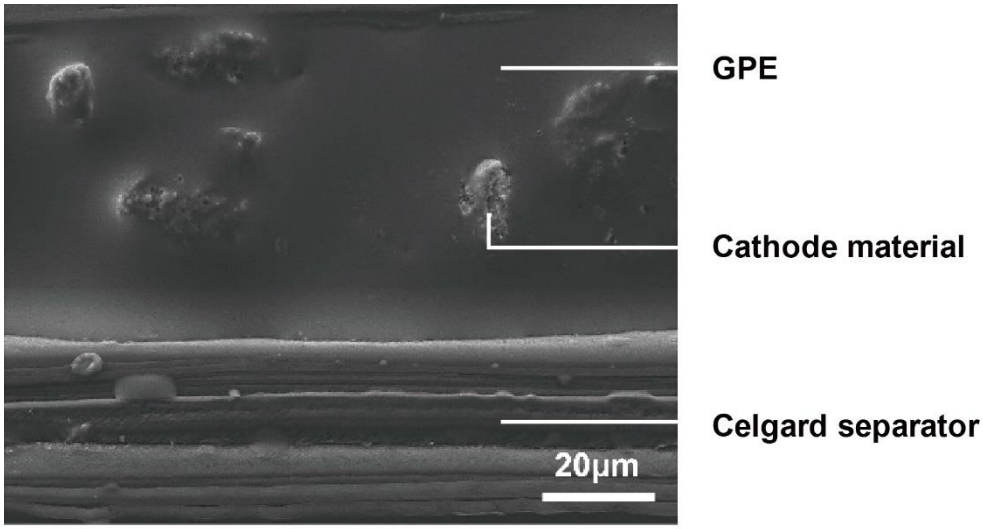

Fig. S14. Cross-sectional SEM image of the as-prepared cathode and separator soaked with GPE.

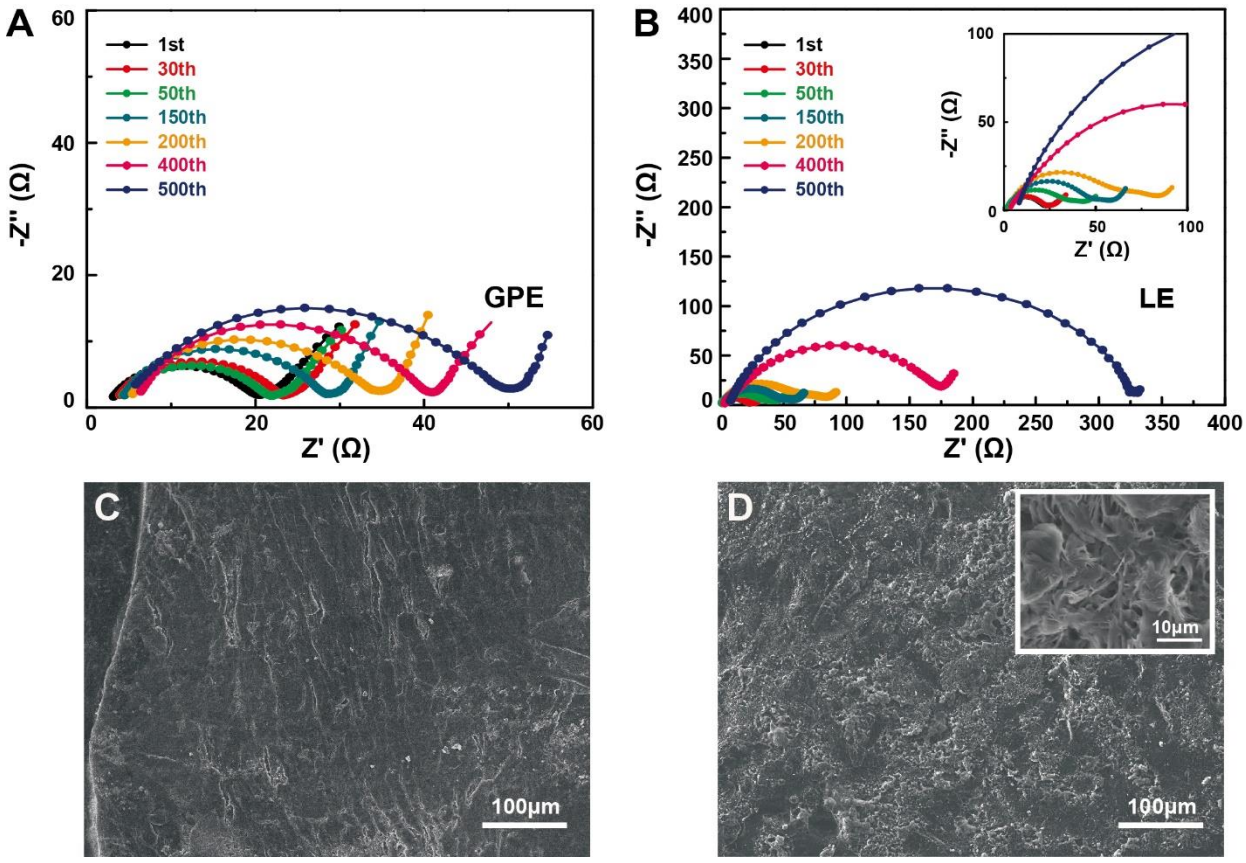

Fig. S15. EIS and anode SEM images of Li-S batteries with GPE and LE. The EIS curves of Li-S batteries under different cyclic intervals (**A**) with GPE and (**B**) with LE at scanning frequency range of 10^{-1}-10^{5} Hz. The surface morphologies of Li anodes in Li-S batteries (**C**) with GPE and (**D**) with LE after 50 cycles at 0.5 C.

The Nyquist profiles are investigated thoroughly within different cyclic intervals (fig. S15, A and B) corresponding to long cycling test presented in Fig. 4E. It can be seen that the resistances of Li-S battery with LE gradually increase among the first 200 cycles, indicating a tougher ionic migration which is responsible for rapid capacity decay. After two drastic leaps at 400 and 500 cycles, the internal resistance grows up to 325 Ω (fig. S15B). In contrast, Li-S battery with GPE holds much less variation of internal resistance that only shifts from 20 Ω to 50 Ω after 500 cycles (fig. S15A), demonstrating an unobstructed ion transition benefitted from the stabilization effect of PDXL-based polymer matrix, which also contributes to the capacity retention.
The Li-S battery using Ketjen black/sulfur as cathode is assembled with *in-situ* gelated GPE, and a battery using the same cathode and DOL/DME LE is also fabricated as the comparison. Both of them are cycled at 0.5 C for 50 cycles and disassembled, and a clear contrast is witnessed by the scanning electron microscope (SEM) characterizations executed on the Li anodes of two batteries after cycling (fig. S15, C and D).

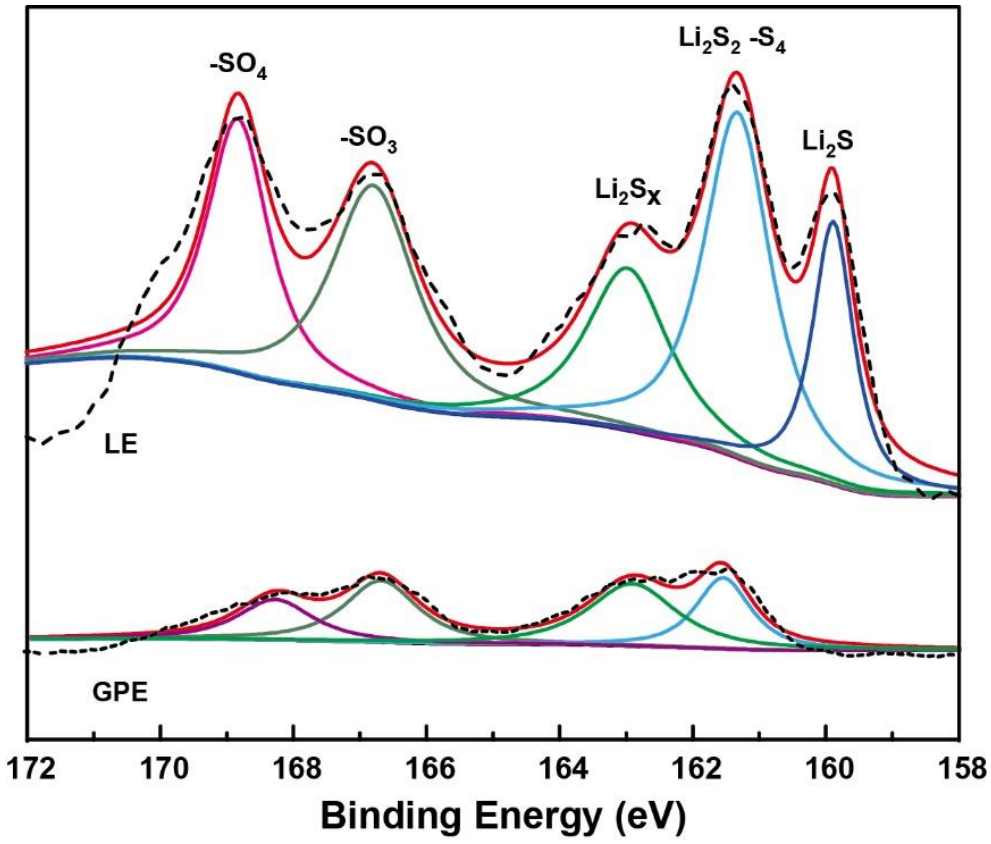

Fig. S16. XPS of the Li anodes of the Li-S batteries with GPE and LE after 50 cycles at 0.5 C.

To verify the reaction products, XPS results obtained for Li anodes with GPE and LE after 50 cycles at 0.5 C in Li-S batteries are demonstrated in fig. S16 . For S 2p spectra, Li_2S_x (163 eV), Li_2S_2-S_4 (161.5 eV) and Li_2S (160 eV) are the products of the reactions between soluble polysulfides and metallic Li. -SO_4 and -SO_3 are deposition products of LiTFSI on the Li anodes. All these chemical species are more sufficient in LE based Li anodes than GPE, indicating severe side reactions between the components in LE and Li than in GPE.

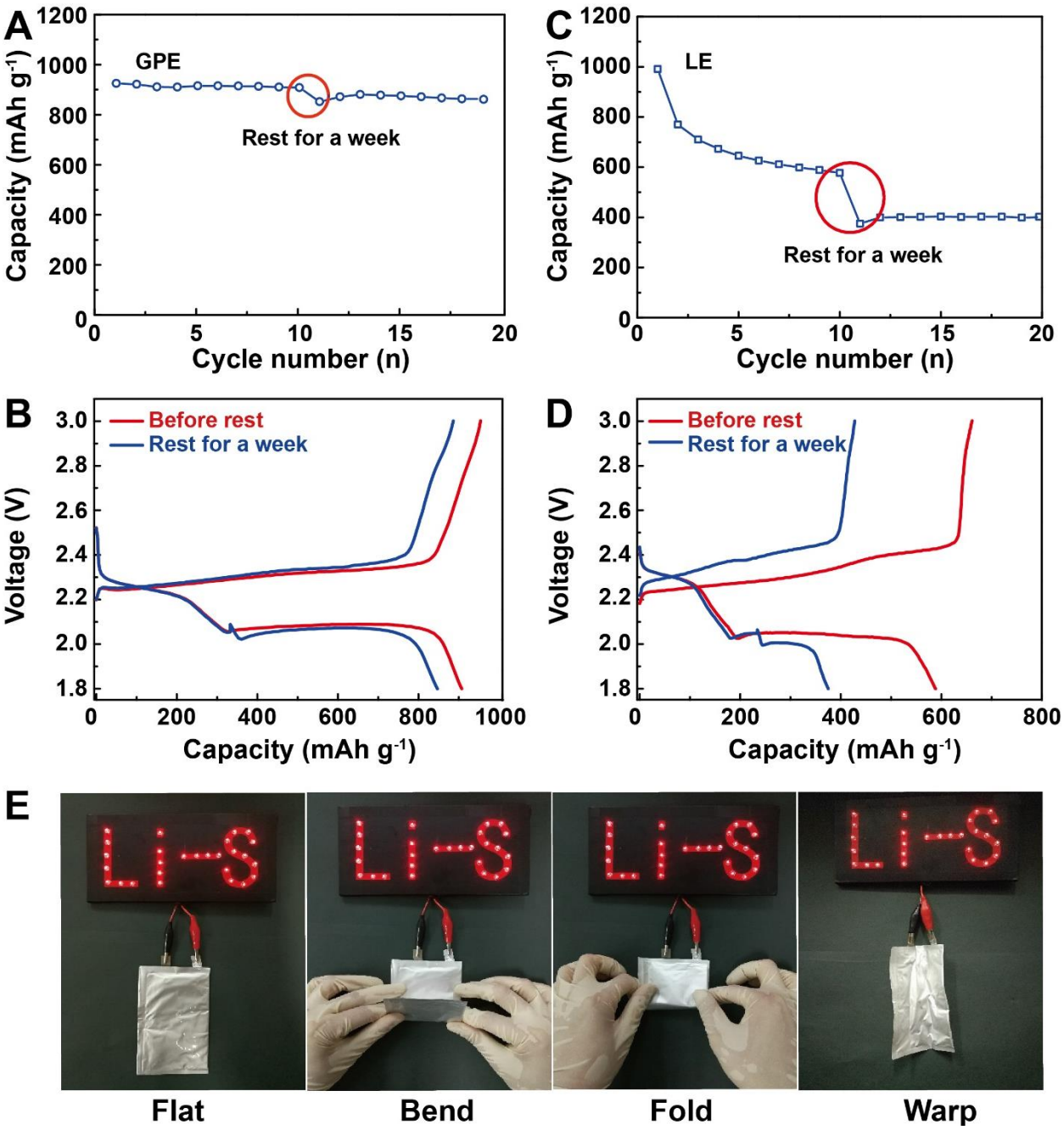

Fig. S17. Self-discharge tests and soft-package Li-S battery. Cycling performance of the batteries (**A**) with GPE and (**C**) with LE. The charge/discharge curves of the 10th and 11th cycles (**B**) with GPE and (**D**) with LE. (**E**) The optical images of LED lamps lighted by flexible Li-S battery with GPE under various mechanical deformation. Photo credit: Feng-Quan Liu, Beijing Normal University.

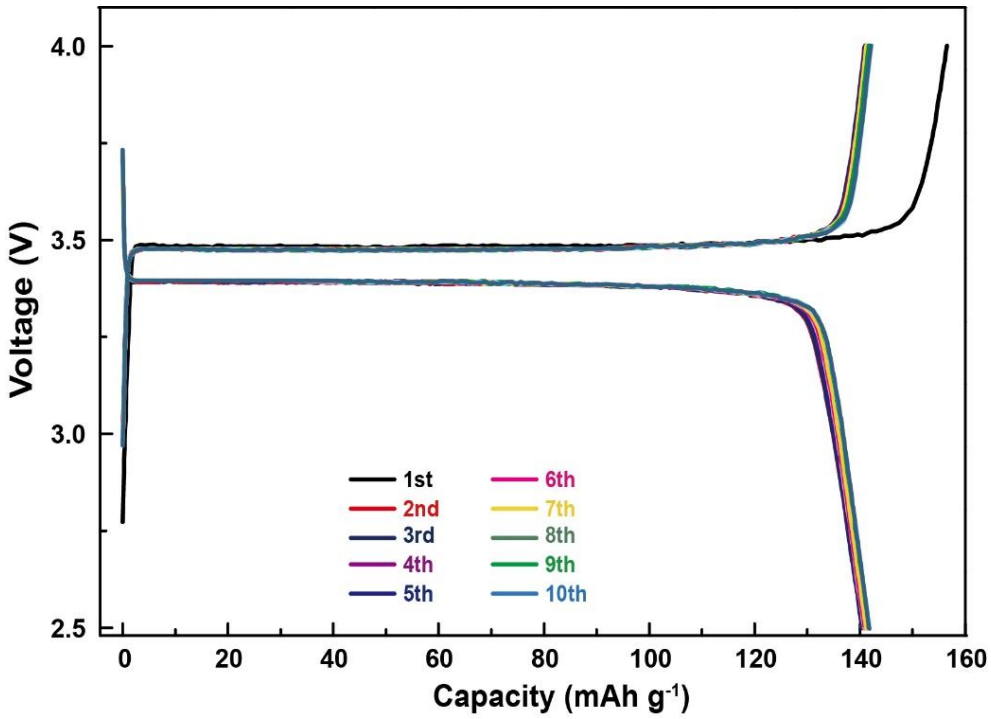

Fig. S18. Charge/discharge curves of $LiFePO_4$|LE|Li battery.

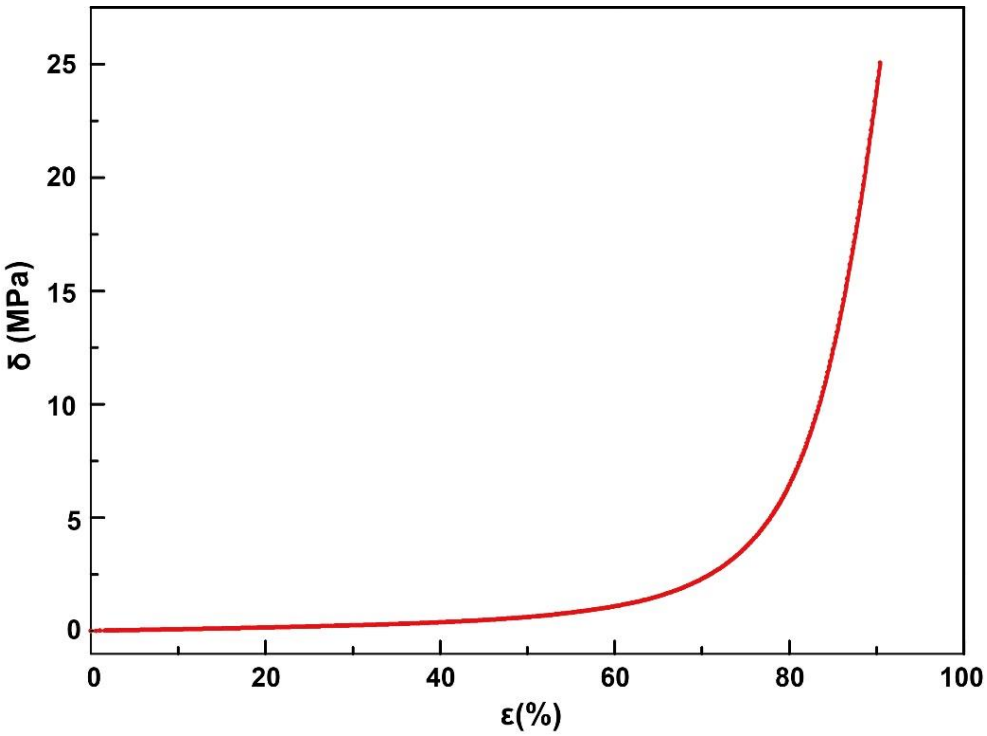

Fig. S19. Mechanical property of GPE with a special shape at room temperature.

Table S1. Polymerization conversion rate of DOL in the electrolyte from monomer to polymer.

Component	Weight (mg)
Liquid electrolyte	1118.23
LiTFSI	287.08
DME	373.60
DOL	457.55
PDXL	416.16

The sample is taken from the gelation of 1 mL liquid electrolyte, which is weighed to be 1118.23 mg, including 287.08 mg LiTFSI, 373.60 mg DME and 457.55 mg DOL. The liquid electrolyte is then added with 2 M $LiPF_6$ for fully polymerization, after which the gel polymer is purified through the two-step method of acetone-dissolution and alcohol-precipitation to remove all the Li salts including LiTFSI and the extra added $LiPF_6$, and the liquid phase containing DME and unreacted DOL, leaving only the PDXL that is weighed as 416.16 mg. Therefore, the percentage of DOL polymerized would be calculated as follow.

$$\text{Polymerization conversion rate} = \frac{\text{m(PDXL)}}{\text{m(DOL)}} = \frac{416.16\ \text{mg}}{457.55\ \text{mg}} = 91.0\%$$

Table S2. Ion conductivity of GPE with various DME content in the precursors.

DME content of precursor	Ion conductivity of GPE ($S \cdot cm^{-1}$)
50%	3.80×10^{-3}
40%	1.85×10^{-3}
30%	5.50×10^{-4}
20%	2.09×10^{-4}